

. 研究成果 (Results)

1. 研究活動 (Research Activities)

掲載論文 Original Papers	88 件
依頼執筆 (研究展望・解説など) Reviews	33 件
口頭発表 Presentations	
国内 Domestic	135 件
国際 International	113 件
プロシーディング Proceedings	
国内 Domestic	60 件
国際 International	90 件
招待講演 Invited Presentations	
国内 Domestic	45 件
国際 International	21 件
特許出願 Patents Application	
国内 Domestic	13 件
国際 International	24 件
特許登録 Patents Registration	
国内 Domestic	8 件
国際 International	12 件

1-1. 論文一覧 (Published Papers)

No	題目 Title	発表者名 Authors	掲載誌 Journals	巻 Vol.	号 No.	頁 Pages
1	True Stress-True Strain Relations at very Low Strain Rates at Room Temperature for an Austenitic 25Cr-19Ni Steel	N. Tsuchida, E. Baba, O. Umezawa, K. Nagai and Y. Tomota	ISIJ International	44	1	209-213
2	In Situ Neutron Diffraction during Tensile Straining of Fine-Grained Ferrite-Pearlite Steel	T. Ono, Y. Tomota, D. Neov, D. Lugovy, P. Lukas, N. Tsuchida and K. Nagai	Materials Science and Technology	20	1	121-125
3	A State of the Art and Development in Materials Process Design and Technology for Sustainable Society	O. Umezawa and K. Nagai	Transactions of the Materials Research Society of Japan	29	5	1925-1930
4	Analysis on Refinement of Columnar γ Grain by Phosphorus in Continuously Cast 0.1 mass% Carbon Steel	N. Yoshida, O. Umezawa and K. Nagai	ISIJ International	44	3	547-555
5	溶接部の漏洩磁束深傷試験に及ぼすHAZの影響 Influence of HAZ on Magnetic Flux Leakage Testing in Weld Zone	梅竹一蔵、長井寿 I. Umetake and K. Nagai	非破壊検査 Journal of The Japanese Society for Non-Destructive Inspection	53	6	358-365

1. 研究活動 (Research Activities)

6	超鉄鋼 Ultra-Steels	長井寿 K. Nagai	日本機械学会論文集 Transactions of the Japan Society of Mechanical Engineers	70	698	1351-1355
7	超微細粒フェライト - セメント鋼の高速引張変形挙動 Tensile Deformation Behavior at High Strain Rate for Ultrafine-grained Ferrite-cementite Steels	土田紀之、 友田陽、 長井寿 N. Tsuchida, Y. Tomoda and K. Nagai	鉄と鋼 Tetsu-to-Hagane	90	12	1043-1049
8	高張力鋼の延性・脆性破壊発生評価手法 Assessment Method of Ductile and Brittle Fracture Initiation in High Strength Steels	榎並啓太郎、 萩原行人、 三村宏 K. Enami, Y. Hagiwara and H. Mimura	日本造船学会論文集 Journal of The Society of Naval Architects of Japan		195	263-269
9	円周切欠引張試験による塑性変形限界の評価 Evaluation of Plastic Deformation Limit by Circumferentially Notched Tension Test	榎並啓太郎、 長井寿 K. Enami and K. Nagai	鉄と鋼 Tetsu-to-Hagane	91	1	285-291
10	Effect of Initial Grain Orientation on Evolution of Deformed Microstructure in Hot Compressed Ni-30Fe Alloy	J. Cho, T. Inoue, F. Yin and K. Nagai	Materials Transactions	45	10	2966-2973

1. 研究活動 (Research Activities)

11	Effect of Shear Deformation on Microstructural Evolution of Ni-30Fe Alloy during Hot Deformation	J. Cho, T. Inoue, F. Yin and K. Nagai	Materials Transactions	45	10	2960-2965
12	A New Evaluation Method of Hydrogen Embrittlement Fracture for High Strength Steel by Local Approach	S. Takagi, S. Terasaki, T. Inoue, K. Tsuzaki and E. Minami	ISIJ International	45	2	
13	Local Approach的手法による高強度鋼の水素割れ感受性評価	高木周作、寺崎聡、津崎兼彰、井上忠信、南二三吉 S. Takagi, S. Terazaki, K. Tsuzaki, T. Inoue and F. Minami	溶接学会論文集 Quarterly Journal of The Japan Welding Society	22	1	125-131
14	MnO-SiO ₂ -FetO系スラグ中りんの熱力学 Thermodynamics of Phosphorus in the MnO-SiO ₂ -FetO System	Y. Kobayashi, N. Yoshida and K. Nagai	ISIJ International	44	1	21-26
15	Effect of Nano-Scale Copper Sulfide Particles on the Yield Strength and Work Hardening Ability in Strip Casting Low Carbon Steel	Z. Liu, Y. Kobayashi and K. Nagai	Material Transactions	45	2	479-487
16	Crystallography and Precipitation Kinetics of Copper Sulfide in Strip Casting Low Carbon Steel	Z. Liu, Y. Kobayashi and K. Nagai	ISIJ International	44	9	1560-1567

1. 研究活動 (Research Activities)

17	Fabrication of High Strength High Nitrogen Stainless Steel with Excellent Corrosion Resistance	Y. Katada, M. Sagara, Y. Kobayashi and T. Kodama	Materials and Manufacturing Processes	19	1	19-30
18	ニアネットシェイプCCにおける鑄造 γ 粒径の予測 Prediction of As-Cast Austenite Grain Size for Near-Net-Shape CC	小林能直、吉田直嗣、長井寿 Y. Kobayashi, N. Yoshida and K. Nagai	鉄と鋼 Tetsu-to-Hagane	90	4	198-205
19	Plastic Anisotropy of Strip-Cast Low-Carbon Steels	P. Xu, F. Yin and K. Nagai	Material Transactions	45	2	447-456
20	Fiber Texture and Substructural Features in the Caliber-Rolled Low Carbon Steels	F. Yin, T. Hanamura, T. Inoue and K. Nagai	Metallurgical and Materials Transactions A	35A	2	665-677
21	Temperature Dependence of Elastic Parameters and Internal Frictions for MnCu ₂₀ Ni ₅ Fe ₂ Alloy	M. Fukuhara and F. Yin	Physica Status Solidi A - Applied Research	201	3	459-466
22	Characteristic Microstructure Features Influencing the Mechanical Behavior of Warm-Rolled Ultrafine Low-Carbon Steels	F. Yin, T. Hanamura, T. Inoue and K. Nagai	Trans MRS-J	29	8	3533-3538
23	Microstructure Control and Wear Resistance of Grain Boundary Allotriomorphic Ferrite/Granular Bainite Duplex Steel	P. Xu, F. Yin and K. Nagai	Materials Science and Engineering A	385	1 and 2	65-73

1. 研究活動 (Research Activities)

24	The Thickness Gradient of Microstructure and Mechanical Property in an As-Cast Thin Steel Slab	P. Xu, F. Yin and K. Nagai	Materials Transactions	45	7	2456-2462
25	Acoustic Characteristics of High Damping $Mn_{73}Cu_{20}Ni_5Fe_2$ Alloy	M. Fukuhara and F. Yin	Physica Status Solidi A - Applied Research	201	3	454-458
26	Electron-Beam-Induced Current Study of Grain Boundaries in Multicrystalline Silicon	J. Chen, T. Sekiguchi, D. Yang, F. Yin, K. Kido and S. Tsuregawa	Journal of Applied Physics	96	10	5490-5495
27	Improvement of Type IV Cracking Resistance of 9Cr Heat Resisting Steel Weldment by Boron Addition	M. Tabuchi, M. Kondo, T. Watanabe, H. Hongo, F. Yin and F. Abe	Acta Metallurgica Sinica	17	8	331-337
28	Ductile-Brittle Transition Temperature of Ultrafine Ferrite/Cementite Microstructure in a Low Carbon Steel Controlled by Effective Grain Size	T. Hanamura, F. Yin and K. Nagai	ISIJ International	44	3	610-617
29	Effect of Aging Treatment on Mechanical Property and H ₂ S Resistant Behavior of Acicular Ferrite Pipeline Steels	M.C. Zhao, Y.-Y. Shan and K. Yang	Acta Metallurgica Sinica	40	9	948-954

1. 研究活動 (Research Activities)

30	Difference in the Role of Non-Quench Aging on Mechanical Properties between Acicular Ferrite and Ferrite-Pearlite Pipeline Steels	M. C. Zhao, T. Hanamura, H. Qiu, K. Nagai and Y.-Y. Shan	ISIJ International	45	1	116-120
31	Fracture Behavior of Ultra-Fine Grained Steel Bar under Dynamic Loading	H. Qiu, Y. Kawaguchi and C. Shiga	Journal of Materials Science	39	11	3733-3737
32	A High-Strength and Low-Yield-Ratio Carbon Steel Bar Processed by Thermo-Mechanical Rolling	H. Qiu, Y. Kawaguchi, C. Shiga, M. Enoki and T. Kishi	Materials Science and Technology	20		1158-1160
33	Strain-Hardening due to Dispersed Cementite for Low Carbon Ultrafine-Grained Steels	A. Ohmori, S. Torizuka and K. Nagai	ISIJ International	44	6	1063-1071
34	Effect of Deformation Temperature and Strain Rate on Evolution of Ultrafine-Grained Structure through Single-Pass Large-Strain Warm Deformation in a Low Carbon Steel	A. Ohmori, S. Torizuka, K. Nagai, N. Koseki and Y. Kogo	Materials Transactions	45	7	2224-2231
35	Effect of Nano-Sized Oxides on Annealing Behaviour of Ultrafine Grained Steels	A. Belyakov, Y. Sakai, T. Hara, Y. Kimura and K. Tsuzaki	Materials Transactions	45	7	2252-2258

1. 研究活動 (Research Activities)

36	Microstructure Evolution in Ferritic Stainless Steels during Large Strain Deformation	A. Belyakov, Y. Kimura, Y. Adachi and K. Tsuzaki	Materials Transactions	45	9	2812-2821
37	Effect of pressing temperature on fine-grained structure formation in 7475 aluminum alloy during ECAP	A. Goloborodko, O. Sitdikov, R. Kaibyshev, H. Miura and T. Sakai	Materials Science and Engineering A	A 381	1-2	121-128
38	Effects of heat and electron irradiation on the melting behavior of Al Si Alloy particles and motion of the Al nanosphere within	J. M. Howe, T. Yokota, M. Murayama and W. A. Jesser	Journal of Electron Microscopy	53	2	107-114
39	Static and in situ TEM investigation of phase relationships, phase dissolution, and interface motion in Ag-Au-Cu alloy nanoparticles	K. Chatterjee, J. M. Howe, W. C. Johnson and M. Murayama	Acta Materialia	52	6	2923-2935
40	Hard metallic glass of tungsten-based alloy	M. Ohtsuki, R. Tamura, S. Takeuchi and T. Ohmura	Applied Physics Letters	84	24	4911-4913
41	Effect of Pass Strain on Grain Refinement in 7475 Al Alloy during Hot Multidirectional Forging	O. Sitdikov, T. Sakai, A. Goloborodko, H. Miura and R. Kaibyshev	Materials Transactions	45	7	2232-2238
42	Microstructure and mechanical properties of Ir-Ta coatings on nickel base single crystal superalloy TMS-75	P. Uppusamis, H. Murakami and T. Ohmura	Journal of Vacuum Science & Technology A	22	4	1208-1217

1. 研究活動 (Research Activities)

43	Effect of Copper on Tensile Properties and Grain-Refinement of Steel and its Relation to Precipitation Behavior	S. Takaki, M. Fujioka, S. Aihara, Y. Nagataki, T. Yamashita, N. Sano, Y. Adachi, N. Nomura and H. Yaguchi	Materials Transactions	45	7	2239-2244
44	Fractional Brownian motion of an Al nanosphere in liquid Al-Si alloy under electron-beam irradiation	T. Yokota, J. M. Howe, W. A. Jesser and M. Murayama	Journal of Applied Physics	95	10	5756-5761
45	Tensile Behavior of TRIP-Aided Multi-Phase Steels Studied by in situ Neutron Diffraction	Y. Tomota, H. Tokuda, Y. Adachi, M. Wakita, N. Minakawa, A. Moriai and Y. Morii	Acta Materialia	52		5737-5745
46	High-resolution transmission electron microscopy study of crystallography and morphology of TiC precipitates in tempered steel	F. G. Wei, T. Hara and K. Tsuzaki	Philosophical Magazine	84	17	1735-1751
47	Precise determination of the activation energy for desorption of hydrogen in two Ti-added steels by a single thermal-desorption spectrum	F. G. Wei, T. Hara and K. Tsuzaki	Matallurgical and Materials Transactions B - Process Metallurgy and Materials Processing Science	35		587-597

1. 研究活動 (Research Activities)

48	Hydrogen absorption of incoherent TiC particles in iron from environment at high temperatures	F. G. Wei and K. Tsuzaki	Metallurgical and Materials Transactions A - Physical Metallurgy and Materials Science	35		3155-3163
49	Response of hydrogen trapping capability to microstructural change in tempered Fe-0.2C martensite	F. G. Wei and K. Tsuzaki	Scripta Materialia	52	6	467-472
50	Hydrogen degradation of a boron-bearing steel with 1050 and 1300 MPa strength levels	M. Wang, E. Akiyama and K. Tsuzaki	Scripta Materialia	52	5	403-408
51	Matrix strength evaluation of ultra-fine grained steels by nanoindentation	T. Ohmura, K. Tsuzaki, N. Tsuji and N. Kamikawa	Journal of Materials Research	19	1	347-350
52	Mechanical characterization of secondary-hardening martensitic steels using nanoindentation	T. Ohmura, T. Hara, K. Tsuzaki, H. Nakatsu and Y. Tamura	Journal of Materials Research	19	1	79-84
53	Evaluation of grain boundary effect on the strength of Fe-C martensitic steels through nanoindentation technique	T. Ohmura and K. Tsuzaki	Materials Science Forum	475-479		4113-4116

1. 研究活動 (Research Activities)

54	Dislocation-grain boundary interaction in martensitic steel observed through in-situ nanoindentation in a TEM	T. Ohmura, A. Minor, E. Stach and J. W. Morris, Jr.	Journal of Materials Research	19	12	3626-3632
55	Effect of inhomogeneity of carbide precipitation on nanohardness distribution for martensitic steels	X. Li, T. Ohmura and F. G. Wei	Materials Science Forum	475-479		4109-4112
56	Radiation-induced swelling and softening in magnesium aluminate spinel irradiated with high-flux Cu-ions	C.G. Lee, T. Ohmura, Y. Takeda, S. Matsuoka and N. Kishimoto	Journal of Nuclear Materials	326	2-3	211-216
57	Variant Selection in Fcc-to-Bcc Precipitation at Grain Boundaries in Ni-43Cr Alloy	Y. Adachi, F. Yin, K. Hakata and K. Tsuzaki	Materials Science Forum	475-479		305-309
58	Recovery and Recrystallization in Cold Worked Fe-O Steels	A. Belyakov, Y. Sakai, T. Hara, Y. Kimura and K. Tsuzaki	Materials Science Forum	467-470		229-234
59	New Grain formation in a Coarse-Grained 7475 Al Alloy during severe Hot Forging	O. Sitdikov, T. Sakai, A. Goloborodko, H. Miura and R. Kaibyshev	Materials Science Forum	467-470		421-426

1. 研究活動 (Research Activities)

60	Geometric Dynamic Recrystallization in an AA2219 Alloy Deformed to Large Strains at an Elevated Temperature	R. Kaibyshev, I. Mazurina and O. Sitdikov	Materials Science Forum	467-470		1199-1204
61	A new method to determine the activation energy for hydrogen desorption from steels	F. G. Wei, K. Tsuzaki and T. Hara	Materials Science Forum	475-479		229-232
62	Origin of the Hydrogen Absorption by Incoherent TiC Particles in Iron	K. Tsuzaki and F. G. Wei	Materials Science Forum	475-479		233-236
63	High-temperature Annealing for Maximization of Dissolved Boron	F. Abe, T. Horiuchi and K. Sawada	Materials Science Forum	426-432		1393-1398
64	Creep Properties and Microstructures on Thermo-Mechanical and Magnetic Treated 9Cr Ferritic Steels	S. Muneki, H. Okubo, H. Okada and F. Abe	Materials Science Forum	426-432		1023-1028
65	Effect of Co Addition on Microstructure in High Cr Ferritic Steels	K. Yamada, M. Igarashi, S. Muneki and F. Abe	ISIJ International	43	9	1438-1443
66	Microstructure and Creep Strength of Welds in Advanced Ferritic Power Plant Steels	F. Abe and M. Tabuchi	Science and Technology of Welding and Joining	22	1	22-30

1. 研究活動 (Research Activities)

67	Effect of Carbon Concentration on Precipitation Behavior of $M_{23}C_6$ Carbides and MX Carbonitrides in Martensitic 9Cr Steel during Heat Treatment	M. Taneike, K. Sawada and F. Abe	Metallurgical and Materials Transactions A - Physical Metallurgy and Materials Science	35A	4	1255-1261
68	MAミリング雰囲気によるガス不純物およびその衝撃強さに及ぼす影響 Gas Contamination Due to Milling Atmospheres of Mechanical Alloying and Its Effect on Impact Strength	村松裕治、 鱈川周治、 太田口稔、 岡田浩一、 阿部富士雄 Y. Muramatu, S. Wanikawa, M. Otaguchi, H. Okada and F. Abe	日本金属学会誌 Journal of The Japan Institute of Metals	68	1	21-26
69	高Crフェライト系耐熱鋼中生成するBN系介在物 BN Type Inclusions Formed in High Cr Ferritic Heat Resistant Steel	櫻谷和之、 岡田浩一、 阿部富士雄 K. Sakuraya, H. Okada and F. Abe	鉄と鋼 Tetsu-to-Hagane	90	10	819-826
70	Influence of Cyclic Strain Rate on Environmentally Assisted Cracking Behavior of Pressure Vessel Steel in High Temperature Water	X. Wu and Y. Katada	Materials Science and Engineering A - Structural Materials Properties Microstructure and Processing	379	1-2	58-71
71	Influence of Strain Rate Change on Corrosion Fatigue Behavior of A533B Steel in Simulated BWR Water	X. Wu and Y. Katada	Journal of Materials Science	39	7	2519-2522

1. 研究活動 (Research Activities)

72	Role of H ₂ O ₂ in microbially influenced ennoblement of open circuit potentials for type 316L stainless steel in seawater	N. Washizu, Y. Katada and T. Kodama	Corrosion Science	46	5	1291-1300
73	Hydrogen-Involved Tensile and Cyclic Deformation Behavior of Low-Alloy Pressure Vessel Steel	X. Wu, Y. Katada, S. G. Lee and I. S. Kim	Metallurgical and Materials Transactions - Physical Metallurgy and Materials Science	35A	5	1477-1486
74	Fabrication of High Strength High Nitrogen Stainless Steel with Excellent Corrosion Resistance	Y. Katada, M. Sagara, Y. Kobayashi, and T. Kodama	Materials and Manufacturing Processes	19	1	19-30
75	Role of Inclusions and Carbide Bands in Corrosion Fatigue of Pressure Vessel Steel in High Temperature Water	X. Wu and Y. Katada	Corrosion	60	11	1045-1057
76	Cyclic Cracking Behavior of Low-Alloy Pressure Vessel Steel in Simulated BWR Water	X. Wu and Y. Katada	Journal of Nuclear Materials	328	2-3	115-123
77	Corrosion Fatigue Behavior of Low-Alloy Pressure Vessel Steels in High Temperature Water Under Multi-Factor Conditions	X. Wu and Y. Katada	Journal of Pressure Vessel Technology - Transactions of the ASME	126	4	466-472

1. 研究活動 (Research Activities)

78	高窒素鋼の創製とその特性 Fabrication of high nitrogen steel and its properties	片田康行、 相良雅之 Y. Katada and M. Sagara	防錆管理 Rust Prevention and Control	48	9	329- 334
79	Localized Corrosion Behavior of High Nitrogen Steel	Y. Katada, N. Washizu, and H. Baba	Materials Science Forum	475- 479		225- 228
80	溶接施行途上の相変態の検出 - レーザースペckルによるひずみ測定法の溶接への適応 (第6報) - Detection of Phase-transformation during Welding Procedure-Application of the Laser Speckle Method to Strain measurement in the Welding Process (report 6) -	村松由樹、 黒田聖治、 山本純司、 金裕哲 Y. Muramatsu, S. Kuroda, J. Yamamoto, and K. You-Chul	溶接学会 論文集 Quarterly Journal of The Japan Welding Society	22	1	101- 106
81	低変態温度材料と残留応力の生成についての考察 - レーザースペckルによるひずみ測定法の溶接への適応 (第7報) - Low Transformation Temperature Materials and Welding Residual Stress-Application of the Laser Speckle Method to Strain Measurement (Report 7) -	村松由樹、 黒田聖治、 山本純司、 金裕哲 Y. Muramatsu, S. Kuroda, J. Yamamoto and K. You-Chul	溶接学会論 文集 Quarterly Journal of The Japan Welding Society	22	1	107- 116

1. 研究活動 (Research Activities)

82	Mechanism Governing Nitrogen Absorption by Steel Weld Metal during Laser Welding	W. Dong, H. Kokawa, S. Tsukamoto, Y. Sato and M. Ogawa	Metallurgical and Materials Transactions B - Process Metallurgy and Materials Processing Science	35B	4	331-338
83	大出力CO ₂ レーザーによる厚板貫通溶接時の凝固割れ発生機構とその抑制 Formation Mechanism and Suppression of Hot Cracking in Full Penetration Welding of Thick Plate using High Power CO ₂ Laser	荒金吾郎、 塚本進、 川口勲、 本田博史 G. Arakane, S. Tsukamoto, I. Kawaguchi and H. Honda	高温学会誌 Jorral of High Temperature Society	30	3	148-153
84	Fracture behavior of ultra-fine grained steel bar under dynamic loading	H. Qiu, Y. Kawaguchi and C. Shiga	Journal of Materials Science	39		3733-3737
85	高張力鋼の延性・脆性破壊発生評価手法 Assessment method of ductile and brittle fracture initiation in high strength steels	榎並啓太郎、 萩原行人、 三村宏 K. Enami, Y. Hagihara and H. Mimura	日本造船学会論文集 Journal of the Society of Naval Architects of Japan		195	263-270

1. 研究活動 (Research Activities)

86	<p>サイドノッチ付シャルピー試験による靱性評価法 Toughness evaluation by Means of Side-Notched Charpy Test</p>	<p>萩原行人、塚本進、大谷忠幸、荒金吾郎、松田鋼 Y. Hagihara, S. Tsukamoto, T. Ohtani, G. Arakane and K. Matsuda</p>	<p>鉄と鋼 Tetsu-to-Hagane</p>	90	7	526-532
87	<p>超狭開先アーク溶接における超細粒鋼熱影響部の特性 Characteristics of HAZ of Ultra-fine grained steel in Ultra-narrow gap GMA welding</p>	<p>伊藤礼輔、平岡和雄、志賀千晃 R. Ito, K. Hiraoka and C. Shiga</p>	<p>溶接学会論文集 Quarterly Journal of The Japan Welding Society</p>	22	3	458-466
88	<p>High-strength and low-yield-ratio carbon steel bar processed by thermo-mechanical rolling</p>	<p>H. Qiu, Y. Kawaguchi and C. Shiga</p>	<p>Materials Science and Technology</p>	20		1158-1160

1-2. 依頼執筆リスト (Reviews List)

No.	著者 Authors	題目 Title	雑誌名・書物 Journals・ Books	巻-号 Vol. -No.	年/月 Date	ページ Pages
1	長井寿 K. Nagai	超鉄鋼材料 - リサイクル鉄の超鉄鋼化 Ultra Steel - Creation of Ultra Steel from Steel Scrap	未来材料 Expected Material for the Future	4-4	2004	41-47
2	長井寿 K. Nagai	未来の金属材料 - スーパーメタル、超鉄鋼など盛んな研究開発 Future Material - Research on Ultra Steel	プラントエンジニア PLANT ENGINEER	36-8	2004	13-17
3	長井寿 K. Nagai	日本やアジアの実状にあった鉄鋼づくりを中小企業とともに - 近未来の鉄鋼材料に挑む Cooperation with SMEs - Challenge for Future Materials	中小商工業研究 Quarterly Small Business Journal	81	2004	126-138
4	長井寿 K. Nagai	安心な生活空間を確保する材料技術 - 構造材料の開発と応用 - Materials Technology to Ensure Safety of Life Space	放送大学用教材 Textbooks of the University of the Air		2004	
5	長井寿 K. Nagai	近未来の鉄鋼材料に挑む - リサイクル鉄を強度・寿命2倍の超鉄鋼に変える Challenge for Future Materials	技術と自然の未来を探る ナノテクから宇宙まで		2004	34-48

1. 研究活動 (Research Activities)

6	川端友弥、 平松秀基、 榎並啓太郎、 島貫広志 T. Kawabata, H. Hiramatsu, K. Enami and H. Shimanuki	特集 構造安全性維持基準の最近のトレンド - T型溶接鋼管における維持基準を利用した破壊評価の例 - Technical Information - Special Issue - Example of Fracture Evaluation of Welded Tubular T-Joint Using Various Failure Assessment Methods	溶接学会誌 Journal of The Japan Welding Society	73-6	2004	447-452
7	井上忠信 T. Inoue	加工ひずみ制御による高効率な結晶粒微細化技術の探索 Search for Highly Effective Crystal Grains Refinement Technology Based on Strain Control	塑性と加工 Journal of the Japan Society for Technology of Plasticity	45-527	2004	1042-1044
8	小林能直、 長井寿 Y. Kobayashi and K. Nagai	鋼中不純物と急凝固組織 Impurities in Steel and Microstructure of Rapid Solidification	まてりあ Materia Japan	43-9	2004	730-736
9	殷福星 F. Yin	制振合金の機能性と応用 The Properties and Application of Damping Alloys	新材料科学及び実用技術		2004	156-175
10	鳥塚史郎 S. Torizuka	超微細組織鋼の創製とその応用 Creation of Ultrafine-grained Steel and its Applications	企業と知的財産 Enterprise and Intellectual Property	387	2004	14-14

1. 研究活動 (Research Activities)

11	津崎兼彰、 三島良直、 熊井真次 K. Tsuzaki, Y. Mishima and M. Kumai	社会基盤材料の材料 戦略概要 R&D Strategy for structural materials	までりあ Materia Japan	43-5	2004/5	384- 387
12	三島良直、 津崎兼彰 Y. Mishima and K. Tsuzaki	革新的機能具現化ブ ロタイピング共同研 究会のあゆみ A new methodology on the materials research for a break-through technology	までりあ Materia Japan	43- 10	2004/ 10	799- 800
13	F. Abe	9Cr-1Mo steel	Creep Properties ; Heat Resistant Steel and Superalloys		2004	118- 125
14	F. Abe	9Cr-2Mo steel	Creep Properties ; Heat Resistant Steel and Superalloys		2004	134- 139
15	F. Abe	12Cr-1Mo-1W-0.3V steel	Creep Properties ; Heat Resistant Steel and Superalloys		2004	161- 169
16	F. Abe	18Cr-8Ni steel	Creep Properties ; Heat Resistant Steel and Superalloys		2004	206- 226

1. 研究活動 (Research Activities)

17	阿部富士雄 F. Abe	18Cr-12Ni-Mo steel	Creep Properties ; Heat Resistant Steel and Superalloys		2004	227-246
18	阿部富士雄 F. Abe	従来材料技術 Conventional Heat Resistant Steels	日本機械学会「石炭利用発電の高効率化技術に関する調査研究分科会」報告書 Technology Issues for Improvement of Efficiency in Coal-fired Power Plants		2004/6	40-52
19	阿部富士雄 F. Abe	高温USC用材料技術 Heat Resistant Materials for Advanced USC Plant	日本機械学会「石炭利用発電の高効率化技術に関する調査研究分科会」報告書 Technology Issues for Improvement of Efficiency in Coal-fired Power Plants		2004/6	119-140
20	片田康行 Y. Katada	高窒素鋼の創製と諸特性 - 物性、加工性、機械的性質 - Fabrication of HNS and Its Properties - Physical Properties, Formability and Mechanical Properties -	ふえらむ Bulletin of The Iron and Steel Institute of Japan (Ferrum)	9-2	2004/2	18-20

1. 研究活動 (Research Activities)

21	片田康行、 相良雅之 Y. Katada and M. Sagara	高窒素鋼の創製と諸 特性 - 窒素添加に よる耐局部腐食特性 とその発現機構 - Fabrication of HNS and Its Properties - Improvement of Localized Corrosion Behavior by N-Alloying -	ふいらむ Bulletin of The Iron and Steel Institute of Japan (Ferrum)	9-2	2004/2	21-23
22	西村俊弥、 小玉俊明 T. Nishimura and T. Kodama	熱力学計算を用いた 新耐候性鋼の耐食指 針提示 Corrosion guidance of new weathering steel by thermodynamic calculation	防錆管理 RUST PREVENTION AND CONTROL	48-4	2004/4	127- 129
23	塚本進 S. Tsukamoto	出力変調レーザ溶接 によるポロシティの抑 制 Suppression of Porosity by Laser welding with Power Modulation.	溶接学会誌 Journal of The Japan Welding Society	73-3	2004/4	145
24	平岡和雄 K. Hiraoka	狭開先溶接 第1回 - 狭開先溶接のねらい - : 低入熱化 - Narrow Gap Arc Welding Process (1) - Technical Aspects of NGW -	溶接技術 Welding Technology	52-5	2004/5	124- 129
25	塚本進、 荒金吾郎 S. Tsukamoto and G. Arakane	貫通レーザ溶接時に 発生するポロシティの 防止 Suppression of Porosity Caused in Full Penetration Laser welding	溶接学会誌 Journal of The Japan Welding Society	73-4	2004/6	204

1. 研究活動 (Research Activities)

26	平岡和雄 K. Hiraoka	狭開先溶接 第2回 - 狭開先化のための技術 開発のポイント - Narrow Gap Arc Welding Process (2) - Technical Aspects of NGW -	溶接技術 Welding Technology	52-6	2004/6	126- 130
27	平岡和雄 K. Hiraoka	狭開先溶接 第3回 - 狭開先溶接の新たな 展開は - Narrow Gap Arc Welding Process (3) - Development of New NGW Technique -	溶接技術 Welding Technology	52-7	2004/7	150- 154
28	本田博史 H. Honda	日本における溶接の 展望 2溶融溶接 (高エネルギー) Review of Welding in Japan	溶接学会誌 Journal of The Japan Welding Society	73-5	2004/7	367- 369
29	T. Nakamura and K. Hiraoka	GMA welding process with periodically controlling shielding gas composition	Guide book 5 "High productivity welding process"	5	2004/7	-66- -71
30	T. Nakamura and K. Hiraoka	Numerical simulation system of development of ultra-narrow Gap GMAW Process	Guide book 5 "High productivity welding process"	5	2004/7	-42- -47
31	中村照美 T. Nakamura	展望 TIG溶接 Review of TIG Welding	溶接学会誌 Journal of The Japan Welding Society	73-5	2004/7	62-63

1. 研究活動 (Research Activities)

32	平岡和雄 K. Hiraoka	狭開先溶接 第4回 - 狭開先溶接とシステム化 - Narrow Gap Arc Welding Process (4) - Development of Automatic NGW System -	溶接技術 Welding Technology	52-8	2004/8	126- 130
33	村松由樹 Y. Muramatsu	レーザスペックルによる ひずみ測定法の溶接への応用 Application of Laser Speckle Strain measurement to a Welding Process	溶接学会誌 Journal of The Japan Welding Society	73-8	2004/ 12	555- 558

1-3. 研究トピックス (Topics)

(a) 冶金グループ (Metallurgical Processing Group)

Topic 1

Improvement of Yield Strength and Work Hardening Ability by Nano-scale Copper Sulfides in Steel

LIU Zhongzhu

E-mail: zzliu@numse.nagoya-u.ac.jp

1. INTRODUCTION

With the steel scrap continuously increasing, the contents of impurities in steel, such as Cu and Sn, increase gradually since they are difficult to be removed during steel making process. In addition, the processes for removing S and P produce a large quantity of slag and expend large amounts of resources and energy. Therefore, inverse utilization of such impurities in steel is of great significance. Direct near net shape casting is an attractive process for the production of sheet metal. Post-treatment like heating and/or rolling is omitted, and the faster solidification rates associated with the direct near shape casting may produce new microstructures. The finer microstructures are generally expected through the faster solidification and cooling rates. This process may have some advantages as one of the future approaches for the efficient utilization of steel scraps because it considers the detrimental effects caused by the impurities in the scraps. In present study, the precipitation behavior of sulfides (manganese sulfide and copper sulfide) in strip casting steel containing 0.11%P-0.01%S-0.07%Cu was investigated. The differences in the mechanical properties between the as-cast and annealed strips were also investigated with an emphasis on the microstructural effects.

2. IMPROVEMENT OF YIELD STRENGTH AND WORK HARDENING ABILITY DUE TO NANO-SCALE COPPER SULFIDES

It was found that the strip casting process not only produced fine microstructures but also resulted in nano-scale copper sulfides. A lot of tiny copper sulfides were observed in the as-cast strips with size less than 50 nm (Fig. 1). The nano-scale sulfides are mainly composed of Cu and S with a little Fe. While in the annealed strips the sulfides are of 100-800 nm. The as-cast strip has higher yield and tensile strengths and maintains high work hardening ability at higher stress levels than that of the annealed strip, as shown in Fig. 2, where TS is tensile strength, YS is yield strength and TS-YS represents the work hardening ability. Both the as-cast and annealed strips have a superior balance of strength and work hardening ability compared with the previous reported strips without the impurities. The nano-scale copper sulfide particles in the as-cast strip contributed most to the difference in the yield strength between the as-cast strip and annealed strips. The as-cast strip also could not produce the good work hardening ability without the nano-size particles. Further improvement in strength and work hardening ability could be attained by controlling the particles' size and the volume fraction in the strip.

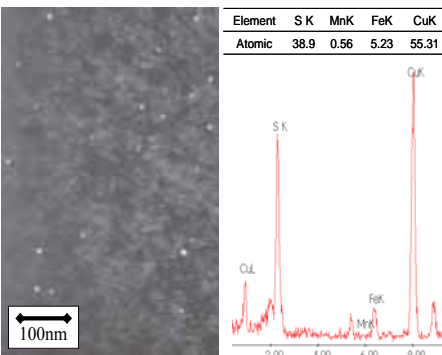


Fig. 1 Nano-scale copper sulfides in present as-cast strips with high impurities.

(a) Dark field, thin foil; (b) EDS, extraction replica.

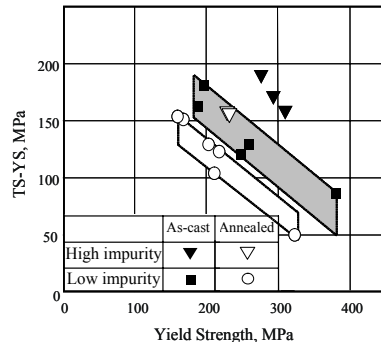


Fig. 2 The yield strength and work hardening ability of present as-cast and annealed strips compared with previous strips with low impurities.

Topic 2

Texture and Formability Evaluation of Strip-Cast Steels

XU Pingguang

E-mail: xupg@mx.ibaraki.ac.jp

1. INTRODUCTION

The solidification rate of strip-casting is about 100 times higher than that of normal continuous casting, and the high solidification rate hence affects the as-cast microstructure extensively. However, rare results have been reported on the microstructure and properties of the as-cast steel under the high solidification rate. In the present work, the strength, ductility, as well as formability of strip-cast low-carbon steel were compared at the as-cast state and the high-temperature annealed state. For the formability evaluation of flat materials, the strain ratio in the thickness direction and the width direction during the tensile experiment of a plate sample, i.e. r -value and the divergence of the r -value with tensile direction, i.e. planar anisotropy Δr , are usually applied.

2. EXPERIMENTAL PROCEDURE

0.05C-0.29Mn-0.12Si (wt.%) steel strip in the dimension of 3mm thick and 600mm wide was produced by a twin-drum strip-caster. The as-cast steel, Sample C, was then annealed at 1473 K for 1.08×10^4 s, and the annealed steel is then called Sample H. Sample C was also cold-rolled to 75% reduction in thickness and then recrystallization annealed at 873K for 1.8×10^4 s (R1) and at 973 K for 1.8×10^3 s (R2), respectively. Tensile tests were conducted with the longitude direction of the tensile samples in 0° , 45° and 90° to the casting direction of the steel strip. The average r -value, $r_m = (r_0 + 2r_{45} + r_{90}) / 4$ and $\Delta r = (r_0 - 2r_{45} + r_{90}) / 2$, as well as the strength and elongation results were obtained for the steel in different treating conditions. The high r -value indicates better formability and the low Δr value means the superior planar anisotropy of the steel strips. On the other hand, X-ray diffraction and scanning electron microscope (SEM) were applied to observe the texture features and ferrite grain distribution in the samples.

3. MICROSTRUCTURE AND PROPERTIES

Sample C shows a tensile strength of 360MPa, which is 40MPa higher than that of Sample H, and a total elongation of 32%. It is indicated that a finer microstructure has been produced during the rapid solidification. Recrystallization annealed samples show not only the higher strength, but also a larger total elongation. Fig 1 shows the average r -value and Δr value of the steel strip in different treating conditions. Samples C combines the higher r -value and lower Δr value, and it is therefore clarified that as-cast steel exhibits a superior strength-formability balance as compared with the annealed steels.

Besides the chemical composition of the steels, the preferred grain orientation of $\{111\}$ on the plate plane and the grain size are also the microstructure features that affect the r -value obviously. With texture analysis, $\{111\}$ and $\{114\}$ orientations on the plate plane are characteristic texture feature in the as-cast steel, and this texture feature is reserved in the post-treating conditions to a certain extent. It is found that the high r -value observed in Sample C could be feasibly attributed to the larger size of the ferrite grains that shows the characteristic orientations. In contrast to the $\{001\}$ oriented grains developed in recrystallization annealed sample, $\{114\}$ texture developed in Sample C and H are considered to cause the lower Δr values.

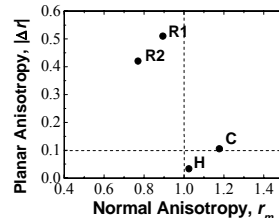


Fig. 1 The r -value and Δr value of the steel in different states

Topic 3

Success in Test Production of Ultra Fine-grained Steel Plate with 35mm Thickness from Scrap Steel

INOUE Tadanobu

E-mail: INOUE.Tadanobu@nims.go.jp

1. INTRODUCTION

Steel is an aggregate of numerous small crystal grains and shows increased strength as the size of these grains decreases. The grain size of steels in general use is 10 μm or more. Steels with grains of 1 μm or less, which is 1/10 of the conventional size, are termed ultra fine grained (UFG) steels. Although ultra fine grain sizes have been achieved in small samples, it was difficult to realize a UFG structure in the material as a whole. In particular, it was considered extremely difficult to produce large-scale UFG samples with existing production capacity. However, in shipbuilding, civil engineering, construction, and other fields, large-scale, high strength steel plates having thicknesses of 25 mm or more with excellent recyclability and resource saving suited to the recycling society of the future had been desired.

2. HOW TO PRODUCE LARGE-SCALE ULTRA FINE GRAINED SAMPLES

To date, the NIMS Steel Research Center has elucidated the principle of ultra grain refinement in basic experiments using very small test pieces (Fig. 1) and attempted to expand this basic principle to test production of large-scale materials. First, several concepts were studied by numerical simulation, and a manufacturing process capable of creating a UFG plate from the viewpoints of the load on the equipment, prediction of the microstructure, and the shape of the plate was proposed. However, a large-scale press and detailed processing technology were necessary in order to verify the new process proposal. Therefore, Muroran Plant of JSW, Ltd. was commissioned to perform the test production work. Using a large-scale press which is part of that company's commercial production equipment, UFG plate of 35 mm in thickness and approximately 90 kg in weight, as shown in Fig. 2, was successfully test-produced by realizing the new process with high accuracy.

3. USE OF SCRAP STEEL

The material used in test production of this plate was a continuous casting slab (produced by Oji Steel., Co., Ltd.) made from scrap steel. Recycling of scrap steel is considered to be important for creating the recycling society of the future and reducing environmental loads not only in Japan, but globally as well. Using the proposed UFG manufacturing process, the possibility of manufacturing UFG steel from scrap steel was demonstrated with commercial production equipment owned by a private-sector company. Among future goals, the Metallurgical Processing Group plans to create larger-scale UFG plates with the aim of realizing use for UFG steels in a variety of fields.

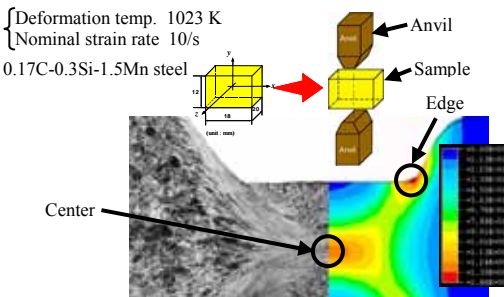


Fig.1 Cross section of compressed sample (lefthand side) and distribution of equivalent strain predicted by numerical analysis (righthand side). Region of large strain corresponds to fine microstructure.



Fig.2 Appearance of test-produced large-scale UFG plate.

Topic 4

Relationship between Effective Grain Size and DBTT among Different Microstructures in Low Carbon Steel

HANAMURA Toshihiro

E-mail: HANAMURA.Toshihiro@nims.go.jp

1. INTRODUCTION

In order to analyze the mechanism of the excellent toughness of ultra-fine steels, the relationship between effective grain size (d_{EFF}) and ductile-brittle transition temperature (DBTT) is investigated for four different microstructures: ultra-fine ferrite/cementite (Uf-F/C), ferrite/pearlite (F/P), quenched (Q), and quenched and tempered (QT). The term "effective grain size" means the fracture unit of a material when it fractures in a brittle manner, such as cleavage fracture. By obtaining the fracture stress (σ_F) from the relationship between d_{EFF} and DBTT, it is found that the value of surface energy determining the fracture stress differs greatly depending on the microstructure. The following equations can be obtained from Pickering's and Griffith's equations, where E is Young's modulus, and A and B constants.

$$\text{DBTT} = A - B \cdot \ln(d_{\text{EFF}}^{-1/2})$$

$$\sigma_F = (4\gamma E/\pi)^{1/2} d_{\text{EFF}}^{-1/2}$$

Based on these equations, it becomes possible to determine surface energy when d_{EFF} and σ_F are determined.

2. EFFECTIVE GRAIN SIZE AND FRACTURE STRESS

Effective grain size is determined to be 8, 20, 100, and 25 μm for Uf-F/C, F/P, Q, and QT. The effective grain size in each microstructure corresponds to a different unit: ferrite grain size for F/P, prior austenite grain size for Q, packet size for QT, and the bigger size in the bimodal distribution of grains for Uf-F/C. The fracture stress is experimentally determined with the assumption that the flow stress at the DBTT of each structure corresponds to its fracture stress. Fig. 1 shows the side view of the cross section of a fracture surface fractured at 77K for each structure. Fig. 2 shows the relationship between d_{EFF} and σ_F . From these figures, it is found that Uf-F/C shows the highest value in fracture stress. This is considered to be due to the fact that the obtained surface energy differs among the four different microstructures that are produced from the same composition. That is, 7.7J/m² for F/P, and 34.6J/m² for Uf-F/C.

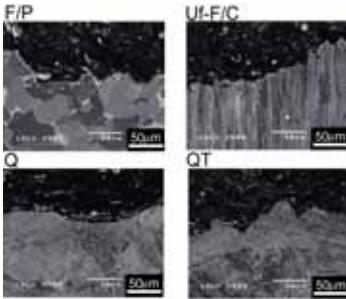


Fig.1 Side view of cross section of fracture surface for each microstructure. The notch is located on the far right and the crack propagated from the right to the left.

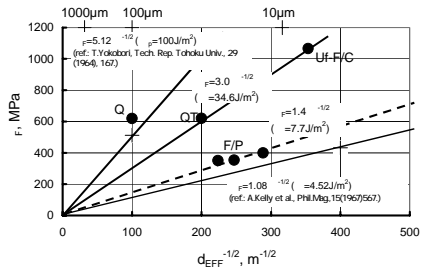


Fig.2 Relationship between fracture stress (σ_F) and effective grain size (d_{EFF}) for each microstructure.

References: T. Hanamura, F. Yin and K. Nagai, ISIJ International, Vol.44 (2004) No.3, 610-617.

(b) 金相グループ (Physical Metallurgy Group)

Topic 1

Measurements of Quick Transient of Repassivation Current after Particle Impact

AKIYAMA Eiji

E-mail: AKIYAMA.Eiji@nims.go.jp

1. INTRODUCTION

Tribocorrosion is an irreversible degradation process of materials resulting from an interaction between mechanical wear and corrosion. Erosion-corrosion is one of the types of tribocorrosion and its typical examples can be seen in pipes and pumps carrying slurry. The kinetics of repassivation on the material surface mechanically damaged by particle impingement is quite important for understanding erosion-corrosion behavior. In this study, rapid transients of small current corresponding to reformation of a passive film on a metal impinged by particles have been measured in order to know the repassivation kinetics and the influence of particle impact on that. Especially, it has been attempted to isolate a single current transient of repassivation caused by a single particle impact.

2. EXPERIMENTAL

The first experimental set up for measuring the current transient caused by a single particle impact was constructed at Max-Planck-Institut fuer Eisenforschung (Duesseldorf, Germany) and a modified set up was built at NIMS. The systems consist of a microelectrode made of a metal wire, a pump gun emitting an aqueous buffer solution containing particles, a potentiostat and a computer equipped with a high frequency data logger. The reasons of the employment of the microelectrode are to reduce background current consisting of passive current and noises, and to isolate single current transients corresponding to single particle impacts by reducing the probability of simultaneous particle impacts on the electrode.

3. RESULTS

Fig. 1 (a) and (b) show an SEM image of zirconia particles for impingement and an AFM image of depressions created by the particle impacts, respectively. An example of a current transient of an Al polarized at 2 V_{Ag/AgCl} in an acetate buffer solution is shown in Fig. 2. As expected, each current peak can be successfully isolated and assigned to a single particle impact. Thus, it has been demonstrated that the setup is useful to evaluate the repassivation behavior. The log-log plot of a current transient shows almost a straight line with a slope of -1. This fact indicates that the reformation of passive film is in accordance with the high field model of oxide growth in which the rate of oxide growth is controlled by ion conduction under high electric field.

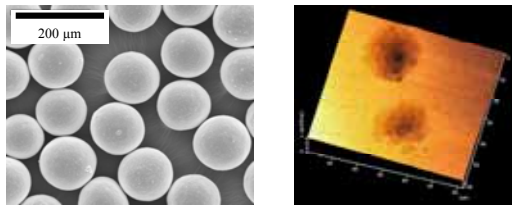


Fig. 1 SEM image of zirconia particles (a) and AFM image of depressions on Al caused by particle impingements.

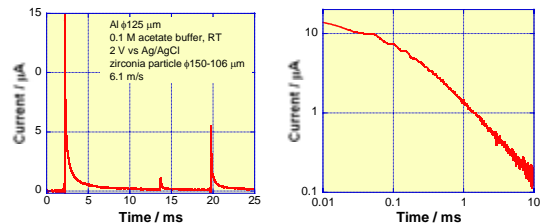


Fig. 2 Current transient of Al caused by particle impingements.

Topic 2

Grain Boundary Effect of Tempered Martensitic Steel Evaluated through Nanoindentation Technique

OHMURA Takahito and TSUZAKI Kaneaki
E-mail: OHMURA.Takahito@nims.go.jp

1. INTRODUCTION

The resistance to deformation transfer from a grain to adjacent grain at a grain boundary is understood as a grain boundary effect corresponding to locking parameter k in the Hall-Petch relation express as:

$$\sigma = \sigma_0 + kd^{-1/2}, \quad (1)$$

where σ is flow stress, σ_0 is constant, k is locking parameter and d is grain diameter. The present study describes the grain boundary effect of Fe-C tempered martensite estimated through nanoindentation technique and considers its relation to microstructures.

2. EXPERIMENTAL

Four nominal carbon contents of 0.2, 0.4, 0.6 and 0.8 mass% were employed. All the specimens were austenitized at 1323 K for 900 s and then quenched. Subsequently, some samples were tempered for 5400 s at various temperatures ranging from 373 to 923 K. The other experimental details are shown in elsewhere [1].

3. RESULTS AND DISCUSSION

Fig. 1 shows the ratio of nanohardness H_n to Vickers hardness H_v (H_n/H_v) plotted as a function of the tempering temperature. The ratio is almost constant below 600K, and increases drastically around 673K. The increase of the ratio indicates a significant reduction of the grain boundary effect, which corresponds to a decrease in the second term in eq. (1). There is no significant difference in grain size of the 573K and 723K tempered specimens [2], hence the change in the term $d^{1/2}$ is denied. Fig. 2 shows bright-field transmission electron micrographs of the Fe-0.4C martensite tempered at (a) 573K, and (b) 723 K. In the case of 573K tempered microstructure, a lot of carbides precipitate on the block boundaries in a film-like state. At the higher tempering temperature at 723 K, a remarkable spheroidization occurs and the film-like carbides on the boundaries disappear. Based on the traditional Hall-Petch model, it is assumed that the film-like carbides have a high resistance to slip transfer. The shear stress τ at the dislocation source in the next grain is expressed as

$$\tau = \alpha \tau_s (L/r)^{1/2}, \quad (2)$$

where α is constant close to unity, τ_s is the average resolved shear stress, L is the distance between the head of the pile-up and the hindward dislocation source and r is the distance from the head of the pile-up to the forward dislocation source in the adjacent grain. When film-like carbides form at the grain boundary, they necessarily enlarge the distance r and shorten the distance L by an amount equal to the thickness of the carbide, hence; the shear stress τ decreases. Therefore, the locking parameter k in eq. (1) is larger for the specimen tempered at 573 K than that for 723 K. Thus, the significant increase of the ratio H_n/H_v , corresponding to the reduction of the grain boundary effect at 723 K is mainly attributed to the disappearance of the film-like cementite on the boundaries.

References:

- [1] T. Ohmura, T. Hara and K. Tsuzaki, *J. Mater. Res.*, **18** (2003) 1465.
[2] T. Ohmura, T. Hara and K. Tsuzaki, *Scripta Mater.*, **49** (2003) 1157.

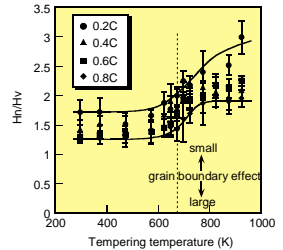


Fig. 1 H_n/H_v plotted as a function of tempering temperature for the Fe-C martensite.

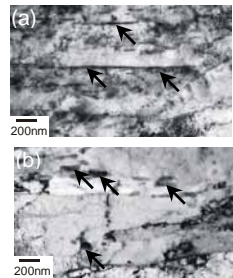


Fig. 2 Bright-field transmission electron micrographs of the Fe-0.4C martensite tempered at (a) 573K, (b) 723 K.

Topic 3

Direct Evaluation of Surface and Interfacial Energies at the Tri-Junction in Two-Phase Nanoparticle by Transmission Electron Microscopy

MURAYAMA Mitsuhiro

E-mail: MURAYAMA.Mitsuhiro@nims.go.jp

1. INTRODUCTION

We present experimental observations and simple analytical calculations which show that the balance among the surface and interfacial energy densities at a three-phase junction and the resulting dihedral angles depend on the relative phase fractions of the solid phases. This result has particularly important implications in nanostructured materials, where phase volumes are small and particles are often able to obtain their equilibrium shape. It also presents a new method to determine the relative values of the surface and interfacial energy densities in two-phase systems, based on the variation of the dihedral angles at the three-phase junction with phase fraction [1].

2. RESULTS AND DISCUSSION

The equilibrium dihedral angles at the solid-solid-vapor tri-junctions of two-phase Cu-Ag alloy nanoparticles 40-100 nm in diameter were measured as a function of phase fraction using transmission electron microscopy. The alloy particles used in this study were formed by thermal evaporation of high-purity Ag and Cu metals from separate tungsten baskets onto heated (520°C) amorphous-carbon TEM grids under high-vacuum (4×10^{-8} Torr) conditions. After evaporation, the grids were held at 520°C for 2 hrs to equilibrate and were then cooled to room temperature in vacuum. The {111} solid-solid interface was cusp-oriented while the surface orientations of the Cu-rich and Ag-rich phases at the tri-junction were largely free to vary. The dihedral angles at the tri-junction were found to vary with the phase fraction, due to the coupling between the amount of each phase and the equilibrium conditions at the tri-junction. This equilibrium condition was used to measure the ratio of the Ag-rich and Cu-rich surface energies to the {111} interfacial energy, which were found as 2.1 and 3.5, respectively. Incidentally, the reasonableness of these results is indicated by comparison of the experimentally determined ratio of the surface energies of Ag to Cu of 0.61, with a ratio of 0.68 based on the average surface energies of pure Ag and Cu, which are 1250 and 1850 mJ/m², respectively, at 0 K. Similarly, the experimental ratio of the interfacial energy to the surface energy of the Cu phase of 0.29 yields a value of 537 mJ/m², based on the average surface energy of pure Cu at 0 K. This is a reasonable value for a partly coherent interface in f.c.c. metals.

References:

[1] J. M. Howe, A. E. Mebed, K. Chatterjee, P. Li, M. Murayama and William C. Johnson, *Acta Mater.*, **51**(2003), 1359-1372.

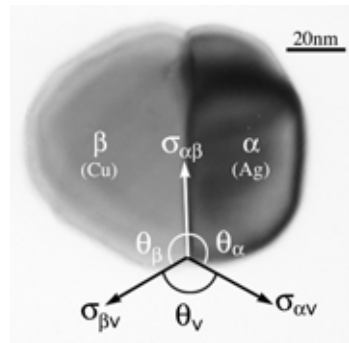


Fig. 1 Bright-field TEM image of a typical two-phase nanoparticle with 60nm in diameter used to measure the dihedral angles, θ_{α} , θ_{β} and θ_v , at the tri-junction. The {111} α/β interface is approximately edge-on in this particle and the surfaces of the α and β phases at opposite ends of the particles display {111} facets parallel to the α/β interface.

Topic 4

Nanohardness Distribution and Its Microstructure Dependence in Tempered Martensitic Steel

LI Jinxu, OHMURA Takahito and TSUZAKI Kaneaki
E-mail: OHMURA.Takahito@nims.go.jp

1. INTRODUCTION

Evaluation of mechanical property in a small scale is essential for understanding mechanical behavior of bulk material. The microstructure of tempered martensitic steel is extremely fine and complex. Therefore, it is important to reveal the relationship between the microstructure and the mechanical property in a sub-micron scale. Nanoindentation technique makes it possible for measuring the mechanical properties in small volumes. In the present work, distribution of nanohardness for a tempered martensitic steel, SCM440 (0.4C-1.12Cr-0.17Mo; tempered at 673K), is evaluated and the relationship between the distribution and the cementite precipitation is discussed.

2. HARDNESS TESTING

Several peak loads from 250 to 2000 μN were applied by using a Berkovich indenter to perform nanoindentation. The standard deviation normalized by average nanohardness were remarkably large of 25.7, 24.7, 15.4 and 14.4 percent corresponding to the loads of 250, 500, 1000 and 2000 μN , respectively. In order to reveal the large distribution of the nanohardness, crystallographic orientation and carbide distribution were considered. Fig.1 shows the nanohardness distribution of (a) the tempered martensite and (b) the sum of the tungsten single crystals with three low surface indices of (001), (101) and (111) tested at 2000 μN peak load. The distribution of the nanohardness for the tempered martensite is much larger than that for the tungsten. This result indicates that the large distribution of the nanohardness of the tempered martensite does not result from the orientation but another factor such as carbide distribution.

3. DISTRIBUTION EVALUATION

In order to clarify if the distribution of cementite particles has effects on the nanohardness distribution, the nanohardness of each indentation was picked out and compared to its location. Fig. 2 shows SEM micrographs taken from some local areas with different density of cementite particles after the nanoindentation test. The density of cementite particles was highest in the area shown in Fig. 2 (a) and lowest in Fig. 2 (c), corresponding to the maximum and minimum average nanohardness of 12.3 and 5.1 GPa, respectively. Fig. 2 (b) represents the area with a moderate cementite density and a moderate nanohardness value of 8.8 GPa. This result indicates that the distribution of the nanohardness is closely related to the distribution of the cementite particles in the deformed zone around the indent.

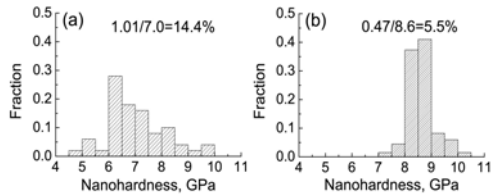


Fig.1 Nanohardness distribution tested at 2000 μN for (a) the tempered martensite and (b) tungsten single crystals in the sum of three surfaces.

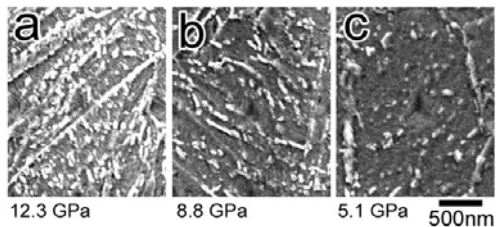


Fig.2 SEM micrographs taken from different local areas with (a) highest, (b) moderate and (c) lowest density of cementite particles for the tempered martensite after the indentation tests at peak load of 500 μN .

(c) 耐熱グループ (Heat Resistant Design Group)

Topic 1

**Improvement of Steam Oxidation Resistance by Formation of Cr_2O_3 Scale
- Initial steam oxidation process of 9Cr ferritic steel -****HARUYAMA Hiroshi****E-mail: HARUYAMA.Hiroshi@nims.go.jp****1. INTRODUCTION**

One of the critical issues for new heat resistant steels towards realization of ultra super critical (USC) power plant, which will be operated at a steam pressure of 35MPa and at a steam temperature of 923K, is the improvement of steam oxidation resistance as well as creep strength. We have previously reported that the protective Cr_2O_3 oxide scale can form on the surface of 9Cr ferritic steel by a combination of palladium addition and surface straining, in spite of insufficient Cr concentration as low as 9%. As a result, oxidation resistance in steam at 923K was significantly improved. However, the forming mechanism of protective Cr_2O_3 oxide scale is little understood. In this study, the initial steam oxidation process of 9Cr ferritic steel containing palladium was investigated by steam oxidation test for the short-duration.

2. EXPERIMENTAL PROCEDURE

Chemical compositions of the steels in this study were based on 9Cr-3W-0.3Si-0.2V-0.05Nb. The concentration of palladium was varied from 0 to 3%. The specimens (20x10x2mm) were ground on 320grit emery paper before oxidation test. The oxidation test was carried out in steam at 650°C for 10min, 1hr, and 10 hr. After the test, the surface oxides were identified by X-ray diffraction. Microstructures of the cross-section were observed by scanning transmission electron microscope equipped with energy dispersive X-ray spectroscopy (STEM/EDS).

3. RESULTS

Fig. 1 shows X-ray diffraction patterns of the surface oxides formed on the specimens oxidized in steam at 650°C for 10hr. Surface oxides formed on the 0%Pd steel were identified as Fe_3O_4 and FeO . The same oxides were also identified at the start of the steam oxidation process; 10min. In the case of 0%Pd steel, these oxides grew into thick double layers. On the other hand, surface oxides formed on the 3%Pd steel were identified as Cr_2O_3 and Fe_3O_4 . Fig. 2 shows the element mapping of the cross-section of the 3% Pd specimen oxidized for 1hr. Thin Cr-rich oxide scale was observed on the surface of the specimen. The thickness of the Cr-rich oxide scale was less than 0.2 μm . This result indicated that the Cr-rich oxide scale was formed in the early stage of steam oxidation process and that the formation of Fe_3O_4 was suppressed.

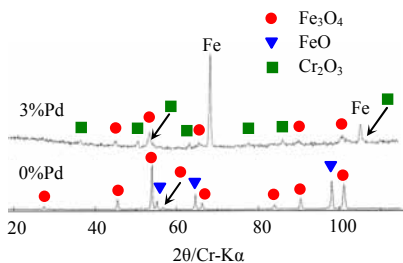


Fig.1. X-ray diffraction patterns of the surface oxides formed on the specimens oxidized in steam at 650°C for 10hr.

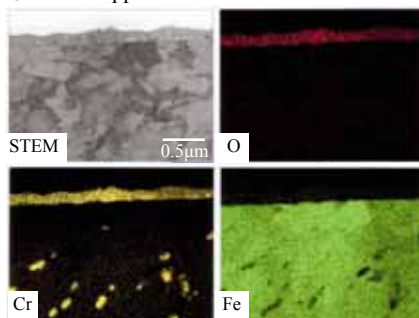


Fig.2. STEM-EDS analysis of the cross-section of the 3% Pd specimen oxidized in steam at 650°C for 1hr.

Topic 2

Application of Magnetic Field to Control the Microstructure of the Heat Resistant Steel

OKUBO Hiroshi and MUNEKI Seiichi
E-mail: OKUBO.Hiroshi@nims.go.jp

1. SCOPE AND OBJECT

Recent trend to utilization of clean energy leading to protection of global environment has been accelerating application of ultra super critical (USC) boilers, which are operated with higher efficiency in power generation than in conventional ones and thus release less amount of carbon dioxide etc. The USC boiler requires heat resistant materials with improved creep rupture strength at elevated temperatures over 923K, because of increase in operating temperature and pressure of the steam used. This study tried to improve the creep strength from the viewpoint of the control of microstructure under magnetic field.

2. IMPROVEMENT OF THE EQUIPMENT

This machine is the worldwide unique prototype equipment. Therefore, the smooth operation was difficult after the equipment introduction. The operation was always enabled by the improvement on thermocouples welding method, microstructure control program and liquid helium filling method, etc...

3. THE CREEP LIFE-IMPROVEMENT BY THE HEAT TREATMENT UNDER MAGNETIC FIELD

The Fe-0.08C-9Cr-3.3W-3.0Co steel was used in this study. Fig.1 compared the creep properties of the base and 3tesla specimens crept at 923K and 120MPa. It became clear that the rupture life of 3tesla specimen was improved in the base and over 3 times from Fig.1(a). The minimum creep rate of 3tesla specimen compared it with the base from Fig.1(b), and it lowered in 1/5. That is to say, it became clear that the creep deformation resistance increased by the heat treatment under magnetic field.

4. CHANGE OF MICROSTRUCTURE BY THE HEAT TREATMENT UNDER MAGNETIC FIELD

Two types of $M_{23}C_6$ carbide and MX carbo-nitride were observed in Fig.2. It is clearly observed that not only grain boundary but also inside the grain $M_{23}C_6$ carbide distributed homogeneously after the heat treatment under magnetic field. In addition, it was also confirmed that MX type carbo-nitride about 10nm in diameter distributed finely from the observation of high magnification of TEM. It is considered that these changes of microstructure regard it as a primary cause of the creep deformation resistance increase.

5. FUTURE EXAMINATION SUBJECT

The ideal microstructure by the application of the heat treatment which included the processing under magnetic field will be researched, while the mechanism which $M_{23}C_6$ carbide and MX nitride make fine dispersion into is examined.

The result of this study was announced in the eighth SAMPE international conference in 2003, and Poster Award was received.

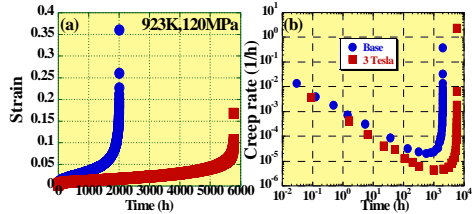


Fig.1 Creep properties of the base and 3tesla specimens crept at 923K under 120MPa.

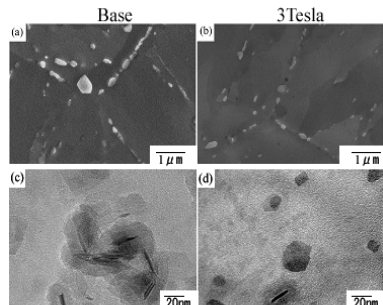


Fig.2 Initial microstructure of the base and 3tesla specimens.

Topic 3

Development of 973K Super Class Ferritic Heat Resistant Steels**- Further challenge of the creep property improvement by carbon-free martensitic alloys -****MUNEKI Seiichi****E-mail: MUNEKI.Seiichi@nims.go.jp****1. SCOPE AND OBJECT**

For global environmental protection, the energy problem which holds the emission of carbon dioxide becomes important more and more. Research and development of heat resistant steel for high-efficient power plant and heat resistant alloy of the 923K super class are widely advanced in Japan, U.S. and Europe. In the carbon-free martensitic alloys, the improvement of the high temperature creep property over 973K becomes possible, and the extension of the application range is expected.

2. PRESENT STATE OF THE STRENGTHENING

Fig. 1 shows relationship between stress and time to rupture of the carbon-free martensitic alloy crept at 973 to 1173K. The fracture time at 973K remarkably increased with the lowering of the stress. Rupture stress at 100,000h is expected with reaching 120MPa, when the gradient of 973K curve is extrapolated. On 973K and 100MPa, it passed through 27,000h, and it was located in the stable creep deformation area. In 80MPa, it has passed through 42,700h, and the test is being carried out. The fracture time at 1023K also similarly increased from 5.7h in 300MPa to about 17,000h in 60MPa with decreasing applied stress. The similar tendency was also shown on 1073K and 1123K. Then, the time at 1173K was also extended to 60MPa for 235.9h from 200MPa for 0.25h. Over test temperature whole area from 973K to 1173K, there was no lowering of the rapid strength on this alloy. It became clear to be the material of which the stress-fracture time relation is very good for this alloy.

3. THE STABILITY BY THE THERMAL CYCLE TEST

The request of the DSS (Daily-Start-Stop) operation heightens in the thermal power plant. Therefore, the improvement in the operability is required in addition to the thermal efficiency improvement in the material. Table 1 shows thermal cycle testing results of type 316 (T316) and the carbon-free alloy (C-free) within 473K and 1273K from 973K by stress loading system by the stroke control. By controlling the tensile stress under holding at the temperature of high temperature side, the deformation which corresponded to the elongation of 1mm from 0.1mm carried out it. The case in which it did not break in the repeat test of 100 times was described with NF. Type 316 austenitic stainless steel broke by the experiment which gave the elongation of 0.5mm and the heating temperature at 1023K in the repetition of 34 times. It broke at 14 times, when the heating temperature was 1073K. The carbon-free martensitic alloy broke at 49 times of the heating at 1173K without breaking for this in 100 time repetition of the same condition as the type 316. It became clear that the carbon-free martensitic alloy also sufficiently resists the severe thermal cycle test like this.

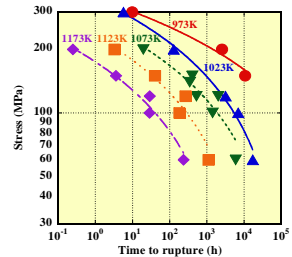


Fig.1 Relationship between time to rupture and stress of the carbon-free alloy.

Table 1 Result of the thermal cycle test.

T 316	0mm	0.1mm	0.5mm	1mm
973K	NF	NF		
1023K	NF	NF	34	
1073K	NF	NF	14	
C-free	0mm	0.1mm	0.5mm	1mm
973K	NF	NF	NF	NF
1023K	NF	NF	NF	NF
1073K	NF	NF	NF	5
1123K			49	
1173K			2	

*It is meant that NF was not broken in the repetition of 100 times. The numeral in the table is number of cycles to the rupture.

Topic 4

Improvement in Creep Strength of Precipitation Strengthened 15Cr Ferritic Steel

TODA Yoshiaki and KIMURA Kazuhiro
E-mail: TODA Yoshiaki@nims.go.jp

1. INTRODUCTION

We have proposed a 15Cr ferritic steel based on ferrite matrix as a new high strength heat-resistant steel which replaces the conventional one. And we have reported that the creep strength and impact toughness of the 15Cr ferritic steel were improved drastically by the optimization of chemical compositions and heat treatment condition. In this study, it is reported that the creep strength of the steel of which impact toughness has been developed could be improved further.

2. DOUBLE STRENGTH AND 1,000 TIMES-LONG LIFETIME

Fig. 1 shows stress vs. time to rupture curves of the furnace cooled (FC) and water quenched (WQ) steels with various contents of Ni at 923K. The curve of the conventional ASME T92 steel is also shown by the dashed curve in the same figure. Regardless of Ni content, the creep strength of the steel was improved drastically by solid solution treatment with water quenching. The creep rupture life of the water quenched 0.4Ni steel was 9,203.6h at 200MPa. The creep strength at 10⁴h of this steel was improved twice as high, and the creep rupture life at 200MPa was extended about 1,000 times as long as that of the conventional one. On the other hand, time to rupture tended to decrease with increase in Ni content among the water quenched steels, and such tendency became remarkable with decrease in stress condition.

3. STRENGTHENING BY HOMOGENEOUS PRECIPITATION OF FINE PARTICLE

Fig. 2 shows SEM images of the water quenched steels with (a) 0.4Ni and (b) 2.0Ni creep ruptured at 923K and 200MPa. t_r values stand for time to rupture. A lot of plate-type fine particles with several hundreds nanometers in size precipitated homogeneously within ferrite matrix in both of the steels and kept fine even after the creep exposure for several thousands hours. On the other hand, martensite phase was also formed in the steel with (b) 2.0Ni. In this steel, austenite phase appeared to be formed at the solution treated temperature of 1473K, and followed by martensitic transformation at low temperature. Coarsened blocky particles with 1 μ m in size were precipitated sparsely within martensite phase. The solid solution treatment with water quenching was significantly effective to improve in the creep strength, because the faster cooling rate than the furnace cooling suppresses the formation of coarse block type precipitates and martensite phase. However, the Ni addition had no effect to extend the creep rupture life. Because Ni is an austenite former element, the Ni addition increased the volume fraction of martensite phase and reduced the precipitation strengthened effect. Consequently, in order to attain further progress in both creep strength and impact toughness of the 15Cr ferritic steel, it is necessary that the formation of martensite phase for the solid solution treated steels with addition of Ni should be suppressed by optimization of chemical composition and heat treatment.

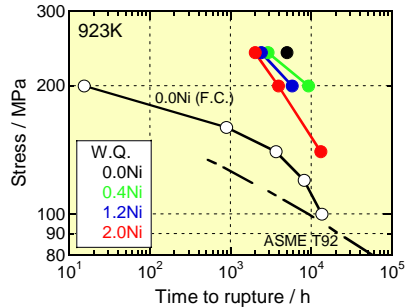


Fig.1 Stress vs. time to rupture curves of the furnace cooled (F.C.) and water quenched (W.Q.) steels with various Ni contents at 923K.

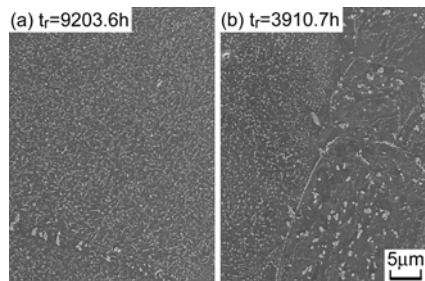


Fig. 2 SEM images of the water quenched steels with (a) 0.4%Ni and (b) 2.0%Ni creep ruptured at 923K-200MPa. t_r stands for the time to rupture.

(d) 耐食グループ (Corrosion Resistant Design Group)

Topic 1

EAC of LWR Structural Materials in High Temperature Water – Corrosion Fatigue of Low-Alloy RPV Steels –

WU Xinqiang and KATADA Yasuyuki
E-mail: WU.Xinqiang@nims.go.jp

1. BACKGROUND

In connection with the light water reactor (LWR) environments various environmentally assisted cracking (EAC) issues should be cautiously considered for the reactor pressure vessel (RPV) and piping system for purposes of safety managements of nuclear power plants, among which corrosion fatigue is of great significance. The higher safety requirements force the development of qualified materials and new strict design criteria to ensure the structural integrity in nuclear power plants throughout their design lives. To meet these requirements, testing of LWR materials under service loading and environmental conditions, data generation, and indication of related EAC mechanisms are a long-term and continuous work. The present attention was mainly paid to the influence of strain rate, thermal aging treatment and sulfur (S) content in steels on fatigue resistance and EAC behavior of low-alloy RPV steels in high temperature.

2. CORROSION FATIGUE RESISTANCE

Fig. 1 shows the effects of strain rate and thermal aging time on fatigue life of the RPV steels. With a decrease in strain rate, the experimental data band moved left gradually from black symbol region to pink symbol region, and then to blue symbol region. This suggested the fatigue resistance of low-alloy RPV steels degrade with a decrease in strain rate in high temperature water. Moreover, the most significant degradation in fatigue resistance was observed for the long-term thermally aged steel or the high S steel in high temperature and high dissolved oxygen (DO) water (asterisks in blue symbol region).

3. EAC BEHAVIORE

Fig. 2 is the typical fatigue cracking and fractographic morphologies of the RPV steels in high temperature water. With a decrease in strain rate, the cracking morphology tended to change from a tortuous manner to an entirely straight manner. Correspondingly the fatigue fracture changed from a quite rough mode to a relatively flat mode. This suggested a strain-rate dependent EAC mechanism dominates the corrosion fatigue process of low-alloy RPV steels in high temperature water.

Further work in corrosion resistant design group in NIMS will be focused on the fatigue safety research of nuclear structural materials (such as pressure vessel and piping steels) in simulated LWR environments as well as the interactive EAC mechanisms among loading conditions, environmental factors and material situations.

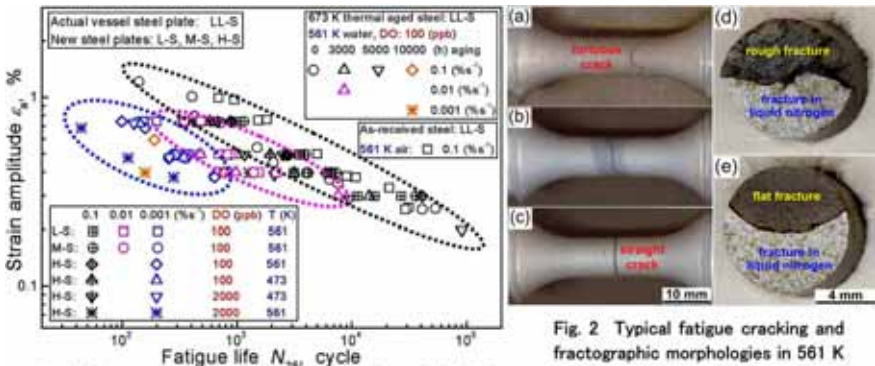


Fig. 1 Low cycle fatigue behavior of RPV steels in high temperature water. LL-S: 0.007wt.%S; L-S: 0.013wt.%S; M-S: 0.025wt.%S; H-S: 0.038wt.%S; Steel: ASTM A533B.

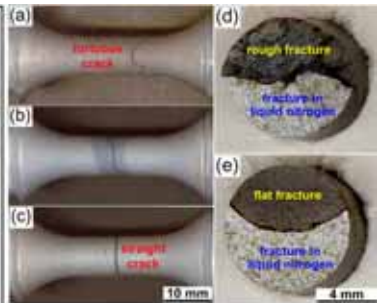


Fig. 2 Typical fatigue cracking and fractographic morphologies in 561 K water at different strain rates, DO: 100 ppb. (a)(d): 0.1%⁻¹; (b): 0.01%⁻¹; (c)(e): 0.001%⁻¹.

Topic 2

Evaluation of Weathering Steel through Accelerated Corrosion Test

KUROSAWA Katsutoshi

E-mail: KUROSAWA.Katsutoshi@nims.go.jp

1. INTRODUCTION

Traditionally, accelerated corrosion tests have been used for quick assessment of the corrosion resistance of steels. However, as the amount of corrosion for weathering steels and carbon steels are almost equivalent, these tests do not accurately reflect the behavior of weathering steels in a natural environment. As an answer to this problem, a new accelerated corrosion test with cyclic periods of moisture and dryness, simulating rainwater washing, has been developed. The relationship between amount of corrosion y and time elapsed in the test x was determined to be $y = Ax^B$, in agreement with results in outdoor.

2. BASIC DATA COLLECTION FOR STANDARDIZATION

Aging time and environment are crucial factors in the formation of an adhered rust layer. In accelerated corrosion tests, the drying period constitutes an important process in rust maturation. Searching for the conditions under which the two types of weathering steels have the highest amount of corrosion, the environmental conditions for the drying period were set at 50% humidity and 50°C of temperature.

Fig. 1 shows the effect of drying time on corrosion for weathering steel. The amount of corrosion has been plotted after 800 hours of testing using the previously showed equation. The actual experiment lasted for 720 hours. The results show that the amount of corrosion is high in the absence of a cycle of water rinsing in 5% NaCl, with a drying period of 6 hours. It is possible to quickly assess the corrosion resistance under these conditions. For a drying period of 6 hours, a strongly adhered rust layer is formed, and there is noticeable difference between the two types of weathering steels regarding the amount of corrosion. The acceleration rate of corrosion decreases with time, similarly as to the case of a natural environment.

3. APPLICATION TO Ni OR Cr DOPED STEELS

Fig. 2 is an example of application to Ni or Cr-added steel of the optimum conditions identified in the previous paragraph. The experiment was carried out twice, and the amount of corrosion for weathering steels (SMA) is shown for comparison. For Ni-added steels, the amount of corrosion decreased as the amount of Ni increased. For Cr-added steels, there was a maximum amount of corrosion in the range of 1 to 5% of addition, but this phenomenon was also observed in outdoor tests, where there is a large amount of chloride ion present. The reason for this phenomenon has not been elucidated.

There was local corrosion in the case of Ni-added steel in the range of 1 to 9%, but for 1% there was general corrosion as time proceeded. For Cr-added steel in the range of 1 to 5%, corrosion changed from local to general corrosion with time, and there was local corrosion for a 9% content.

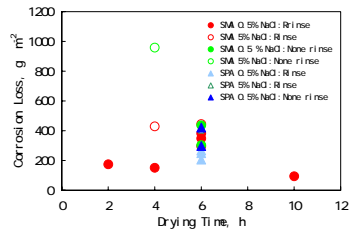


Fig.1 Effect of drying time on corrosion (Salt spray 0.5h + Dry Xh + Wet 1.5h (or Wet 1h + Rinse 0.5h))

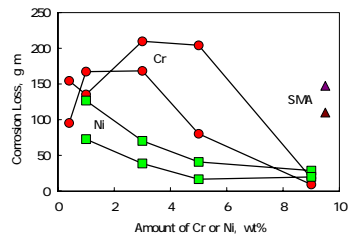


Fig.2 Effect of Ni or Cr addition on corrosion (Salt spray 0.5h + Dry 6h + Wet 1h + Rinse 0.5h)

(e) 溶接グループ (Welding Metallurgy Group)

Topic 1

Detection of Strain Behavior in Low Transformation Temperature Material during Welding

MURAMATSU Yoshiki

E-mail: MURAMATSU.Yoshiki@nims.go.jp

1. INTRODUCTION

Phase-transformation influences strongly on the welding residual stress distribution. The low transformation temperature materials developed in NIMS are effective on reduction of tensile residual stress. It is difficult, however, to detect their transformation behavior experimentally because their M_f temperature is near the room temperature. Moreover, in actual welding procedure, the material is diluted with base plate and depends on stress history, therefore its transformation is accelerated or its M_s temperature rises up. In such case, the laser speckle strain measurement characterized with non-contact and high responsibility is available for these cases in a weld.

2. EXPERIMENTAL PROCEDURE

We used several rectangle thin specimens for the purpose mentioned above. Some 500Mpa class steel specimens have a groove filled up with low transformation temperature materials developed in NIMS in their center position. GTA heating are applied on the center lines of these specimens and apparent strains on the center of specimens are detected using the laser speckle method. Fig. 1 shows the layout of detection by the method.

3. RESULTS

Fig. 2 shows the temperature-strain curves in cases of 9%Ni steel plate and two kind of low transformation temperature material plates during their transformation period. Full S-curve was detected clearly even if the finishing temperature (M_f) is near the room temperature. When the filler made from these materials are diluted with base plate, their transformation temperature will rise. The method is also available in these case as shown in Fig. 3. In this figure, each filler material was diluted with 500Mpa class base plate and the M_s temperature rise above the values in Fig. 2.

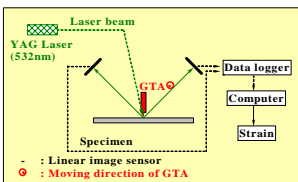


Fig.1 Layout of laser speckle strain measurement.

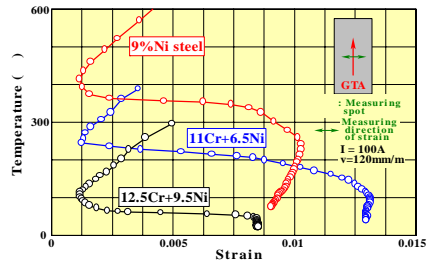


Fig.2 Temperature-strain curves during transformation period.

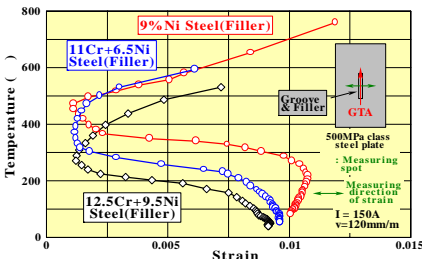


Fig.3 Temperature-strain curves in weld metal.

The laser speckle method can detect dynamic strains directly from any parts of weld during procedure. These data will be important parameters of computing estimation for residual stress distribution or deformation in welded joints.

Topic 2

Welding of Thick Plate by Ultra-Narrow Gap Arc Welding

NAKAMURA Terumi and HIRAOKA Kazuo
E-mail: NAKAMURA.Terumi@nims.go.jp

1. INTRODUCTION

An Ultra-Narrow Gap Arc Welding process has been developed in order to weld thick plate (the plate thickness: 25 mm). The arc heat is distributed by a periodic oscillation of the arc generating points along the groove wall. As a result, the small heat input welding of thick plate becomes possible, because the line heat source is obtained by the arc oscillation.

2. ULTRA-NARROW GAP ARC WELDING PROCESS

The relationship between the total welding heat input and the grooves area is shown in Fig. 1 (the plate thickness: 25 mm). The welding conditions of thick plate are selected by two methods. The one is to secure the large amount of wire melting (Deposition type), and the other is to secure the deep penetration (Penetration type). In the former, the amount of heat input is proportional to the groove area. Small heat input welding becomes possible in narrow grooves. In the latter, it is considered that the formation of penetrating is more important than that of wire melting. The heat input of 11000J/mm or more is necessary to do the submerged arc welding for 25mm in thickness plate and the heat input does not depend on the groove area.

On the other hand, the small heat input process becomes possible by reducing groove area in 'Penetration type'. Then, we developed UNGW process for thick plate.

Welding process in which wire feed rate is controlled synchronizing with pulse current waveform is used in order to disperse arc heat input widely. To reinforce the digging action by the arc, and to secure a steady melting of the bottom, the pulse of about 100Hz was superimposed to the base current. These welding conditions were made proper with a developed welding process simulator.

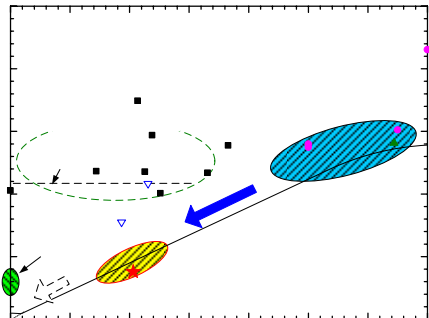


Fig.1 The relationship between heat input and groove area at thick plate.

3. RESULTS

The results of Ultra-Narrow Gap Welding (UNGW) for 25mm plate are shown in Fig. 2(a). The amount of a total heat input of UNGW was able to be decreased to the same level of laser welding (Laser welding: Fig. 1 (a), UNGW: Fig. 1 (c)). In addition, the full penetration weldings were enabled for fillet weld joint (Plate thickness: 19mm).

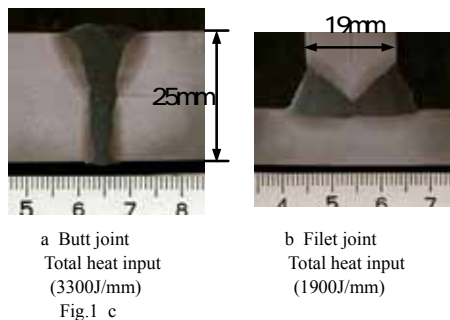


Fig.2 Results of UNGW for thick plate.

Topic 3

Suppression of Type IV Failure by High Boron Addition in 9Cr Steel

KONDO Masayuki, TSUKAMOTO Susumu, TABUCHI Masaaki, and ABE Fujio
E-mail: TSUKAMOTO.Susumu@nims.go.jp

1. INTRODUCTION

Realizing the ultra super critical (USC) boilers to be operated at 923K and above calls for use of new high Cr steels that can withstand high temperatures and pressures in these plants. However, the Type IV failure occurs in the fine grained heat affected zone (HAZ) of the high Cr heat resistant steels welded joints. Due to this, creep lives of the welded joints are much shorter than those of the base metals. New high-B low-N 9Cr steel has been developed at NIMS. High boron content is expected that the welded joint of this steel shall have improved resistance to Type IV failure, according to Type IV failure mechanism revealed by ultra-steels project 1st phase. The purpose of this study is to suppress of Type IV failure in 9Cr steel welded joints, and to improve creep lives of the welded joints.

2. CREEP LIVES OF HIGH-B LOW-N 9Cr STEEL WELDED JOINTS

130ppmB-15ppmN 9Cr steel welded joints were prepared from plates by using gas tungsten arc welding (GTAW) process and Inconel-type filler wire (AWS ER Ni Cr-3). No weld defect was observed and the welded joints successfully passed the side bend tests, in spite of their higher B contents. Fig.1 shows the results of creep rupture tests for the welded joints of 130ppmB steel and P92, respectively. Due to Type IV failure, creep lives of P92 welded joints show much shorter than those of the base metal at low stress level. However, no type IV failure has been observed during the creep rupture tests at 923K conducted on the welded joints of 130ppmB steel for up to about 10000h. Creep lives of 130ppmB steel welded joints are comparable to those of the base metal, and are also longer than those of P92 base metal.

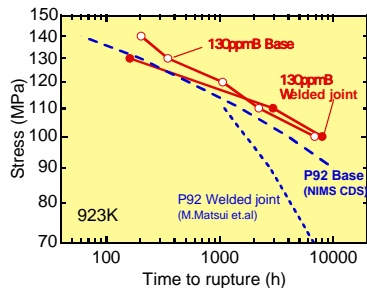


Fig.1 Creep lives vs. applied stress of 130ppmB steel welded joints.

3. LARGE GRAINED HAZ MICROSTRUCTURE

Fig. 2 shows so-called inverse pole figure (IPF) maps with grain boundary mapping of 130ppmB steel welded joints and P92 steel welded joints by EBSD analysis. 130ppmB steel does not have fine grained HAZ at a distance of 1.5mm from the fusion line, while P92 has fine grained HAZ at this location. Here, most of the grains have the same size as the base metal in 130ppmB steel. Inside the large grains, the microstructure shows lath martensite. Large grained HAZ microstructure is one of the probable reasons for suppressing the Type IV failure and improving the creep resistance of the welded joints in the boron steel. To reveal formation mechanism of the large grained microstructure, we need further investigation.

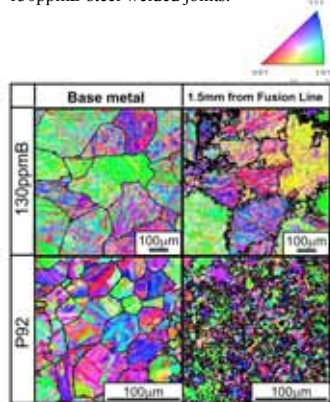


Fig.2 EBSD analysis results of 90ppmB steel and P92 steel HAZ microstructures.

Topic 4

Softening Behavior in Ultra-fine Grained Steel Welds

HIRAOKA Kazuo

E-mail: HIRAOKA.Kazuo@nims.go.jp

1. INTRODUCTION

Ultra-Fine Grained Steels (UFG steels) were produced by finish rolling at 773K with heavy reduction and that their microstructures consisted of ferrite grains of about $1\mu\text{m}$ and uniformly dispersed fine spherical cementite between 0.14 and $0.16\mu\text{m}$. When the UFG steel is welded, fine ferrite grains are coarsened resulting in remarkable softening in the heat-affected zone.

We have focused on elucidation of the metallurgical factors determining hardness of UFG steel HAZ under the welding condition that the arc energy was approximately 1.5kJ/mm in ultra-narrow gap welding process.

2. Results and Discussion

Figure shows the relationship between hardness and the average ferrite grain diameter, d (solid line) at HAZ until $1,300\text{K}$. The fine dotted line in the figure is taken from the result of the ferrite-cementite type of UFG steel by Torizuka et al.²⁾

Fine grained ferrite begins to grow above 920K below A_{C1} and ferrite grains continue to coarsen above the A_{C1} temperature.

Cementite remains untransformed in the HAZ of the UFG steel until peak temperature reaches A_{C1} , while ferrite grains coarsen slightly. From the interpretation that hardness until A_{C1} depends mainly on ferrite grain size, the relationship between average diameter of ferrite grain and hardness was drawn in the broken line. Hardness given by this line is lower than that by Torizuka et al. shown by the fine dotted line.

The UFG steel was produced by the concentrated reduction of rolling and high dislocation density resulted in the UFG steel. Therefore, dislocations are more likely to annihilate in the UFG steel due to welding heat than the ferrite-cementite type of UFG steel. This is considered for the reason of the difference between the fine dotted line and the broken line in the figure.

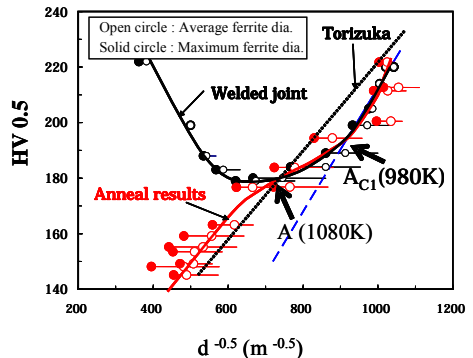
Heat treatment was carried out to the ferrite-cementite type of UFG steel under the several conditions of holding temperature below A_{C1} (960K , 910K or 820K) and holding time ($10 \sim 3600\text{s}$). From these results, the relationship between hardness and ferrite grain size was found as shown with red line in the figure.

Actual hardness of HAZ heated over point A ($1,080\text{K}$) is higher than that predicted only ferrite grain size without M-A constituents, which is given by the red line in the figure.

The difference shows that the second-phase effect through the transformation of cementite to M-A does not appear from A_{C1} to around $1,080\text{K}$ but this effect begins to appear from $1,080\text{K}$.

1) Ito et al: Quarterly J. JWS, Vol.22 (2004), No.3

2) Torizuka et al : CAMP-ISIJ, Vol. 12(1999), p365-368.



Relationship between ferrite grain diameter and Vickers hardness in welded joint of steel UFG

Spiking Phenomenon of Keyhole on Laser Welding

HONDA Hiroshi

E-mail: HONDA.Hiroshi@nims.go.jp

1. INTRODUCTION

High power laser has been expected to be a high efficiency tool to make high quality welds of thick steel plates. One of the problems is weld defects such as porosity. The porosity formation is related to keyhole depth fluctuation called spiking phenomenon. Fig. 1 shows a series of X-ray transmission images near a keyhole tip. Keyhole depth fluctuation was observed. When the keyhole becomes shallower, the keyhole collapses near the keyhole tip and a bubble is formed. The formed bubble goes backward with the molten metal flow and remains as porosity.

To understand the spiking phenomenon, X-ray transmission images of keyhole and light emission images of plume plasma were obtained.

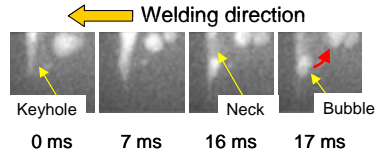


Fig. 1 A series of X-ray transmission images of bubble formation near keyhole tip.

2. INFLUENCE OF BEHAVIOR OF THE UPPER PART OF KEYHOLE

Bead-on-plate welding of mild steel was carried out with CW CO₂ laser system. The laser power was 20 kW and the welding speed was 2 m/min. As a result, it was found that behavior of the upper part of the keyhole affects the plasma plume generation and the spiking phenomenon.

Obtained results are shown in Fig. 2. From the series of X-ray transmission images, it was observed that the upper part of keyhole fluctuates violently. A slender keyhole is observed in Fig 2 (a). In Fig. 2 (b), a swelling appears at the upper part of the keyhole and the molten metal is pushed up to the specimen surface (the pushed molten metal is indicated by the yellow circle). In Fig. 2 (c), the swelling becomes larger and the pushed molten metal is about to close the keyhole entrance. At this time, the plume plasma becomes larger. Therefore, it is supposed that the large plume plasma is generated by the interaction between the incident laser light and the pushed molten metal. After that, the keyhole entrance opens widely and the keyhole deepens (Fig. 2 (d)). It seems that a strong recoil pressure caused by the interaction between the incident laser light and the pushed molten metal pushes the molten metal and open the keyhole entrance widely. In Fig. 2 (e), the keyhole reverts to a slender shape. The behavior on the upper part of the keyhole relates to the spiking phenomenon in this manner.

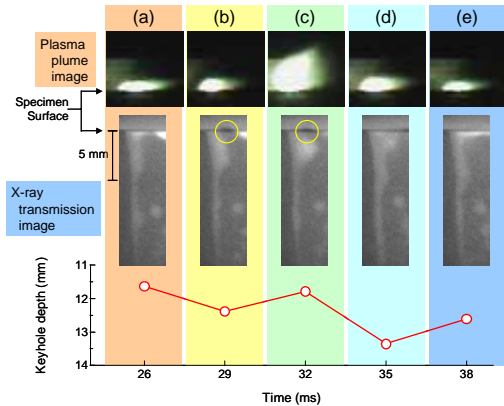


Fig. 2 Observed Plasma plume images, X-ray transmission images, and keyhole depths.

2. 受賞一覧 (Awards)

受賞年月日	授与機関	受賞の名称	氏名(所属)	受賞の理由及び対象論文
2004/3/30	(社)日本鉄鋼協会	澤村論文賞	吉田直嗣 (現住友金属工業株)、梅澤修 (横浜国立大学)、長井寿 (冶金グループ)	Influence of phosphorus on solidification structure in continuously cast 0.1 mass% carbon steel
2004/3/30	(社)日本金属学会	功績賞	鳥塚史郎 (冶金グループ)	
2004/5/22	(社)日本塑性加工学会	新進賞	井上忠信 (冶金グループ)	加工ひずみ制御による高効率な結晶粒微細化技術の探索
2004/10/22	(社)日本機械学会	優秀講演表彰	戸田佳明 (耐熱グループ)	Improvement in Creep Strength of Precipitation Strengthened 15Cr Ferritic Steel by Controlling of Carbon and Nitrogen Contents
2004/11/6	(社)日本機械学会	機械材料・材料加工部門 部門一般表彰 (新技術開発部門)	片田康行 (耐食グループ)	高窒素ステンレス鋼の開発とその展開
2004/11/15	(社)溶接学会	溶接構造シンポジウム 2004 シンポジウム奨励賞	目黒奨 (溶接グループ)	ESPI システムの溶接への適用

3. 学位取得一覧 (Doctor Degrees Qualified)

取得年月日	授与機関	学位の名称	氏名(所属)	学位取得論文題目
2004/3/25	北海道大学	博士(工学)	堀内寿晃 (現㈱日立製作所)	フェライト系耐熱鋼におけるFe-Pd基L10型規則相の相安定性に及ぼすNiの効果の現象論的計算
2004/3/31	Imperial College (英国)	Ph. D.	仙波潤之 (耐熱グループ)	Creep Modelling of Microstructurally Unstable Martensitic Steels
2004/4/15	東京大学	博士(工学)	大森章夫 (現JFEスチール㈱)	超微細フェライト組織鋼の創製と機械的特性の制御に関する研究